BIG DATA MINING AND ANALYTICS
ISSN 2096-0654 03/07 pp84–93
Volume 4, Number 2, June 2021
DOI: 10.26599/BDMA.2020.9020012

Diagnosis of COVID-19 from Chest X-Ray Images Using Wavelets-Based Depthwise Convolution Network

Krishna Kant Singh and Akansha Singh*

Abstract: Coronavirus disease 2019 also known as COVID-19 has become a pandemic. The disease is caused by a beta coronavirus called Severe Acute Respiratory Syndrome Coronavirus 2 (SARS-CoV-2). The severity of the disease can be understood by the massive number of deaths and affected patients globally. If the diagnosis is fast-paced, the disease can be controlled in a better manner. Laboratory tests are available for diagnosis, but they are bounded by available testing kits and time. The use of radiological examinations that comprise Computed Tomography (CT) can be used for the diagnosis of the disease. Specifically, chest X-Ray images can be analysed to identify the presence of COVID-19 in a patient. In this paper, an automated method for the diagnosis of COVID-19 from the chest X-Ray images is proposed. The method presents an improved depthwise convolution neural network for analysing the chest X-Ray images. Wavelet decomposition is applied to integrate multiresolution analysis in the network. The frequency sub-bands obtained from the input images are fed in the network for identifying the disease. The network is designed to predict the class of the input image as normal, viral pneumonia, and COVID-19. The predicted output from the model is combined with Grad-CAM visualization for diagnosis. A comparative study with the existing methods is also performed. The metrics like accuracy, sensitivity, and F1-measure are calculated for performance evaluation. The performance of the proposed method is better than the existing methodologies and thus can be used for the effective diagnosis of the disease.

Key words: coronavirus; COVID-19; deep learning; convolution neural network; X-Ray images

1 Introduction

A pandemic is an outbreak of a disease globally affecting many populations. The world has witnessed many pandemics in the 20th century. Flu viruses are the major cause of pandemics. These viruses show changing behaviour with the changing seasons and thus their behaviour needs to be predicted for prevention. Health professionals generally make the correct predictions about most viruses. But some viruses have exceptional behaviour and are difficult to predict. Such viruses cause pandemics as humans do not have the immunity to resist to such virus.

The latest coronavirus disease known as COVID-19 has appeared and spread extremely fast. Since its discovery in December 2019 in Wuhan, China, the disease has already spread over 199 countries and territories. The Severe Acute Respiratory Syndrome Coronavirus 2 (SARS-CoV-2) causes COVID-19[1]. The virus is a Ribonucleic Acid (RNA) virus from the Coronavirus family, most viruses from this family cause common cold. The more severe variety of coronaviruses is Severe Acute Respiratory Syndrome Coronavirus (SARS-CoV) and Middle East

• Krishna Kant Singh is with Department of ECE, KIET Group of Institutions, Delhi-NCR, Ghaziabad 201206, India. E-mail: krishnaiitr2011@gmail.com.
• Akansha Singh is with Department of CSE, ASET, Amity University Uttar Pradesh, Noida 201310, India. E-mail: akanshasing@gmail.com.
* To whom correspondence should be addressed.
Manuscript received: 2020-06-05; revised: 2020-07-19; accepted: 2020-07-28

Respiratory Syndrome Coronavirus (MERS-CoV). COVID-19 causes respiratory ailments ranging from common cold to serious diseases like pneumonia. The number of cases worldwide has reached 5 817 385 causing the deaths of 362 705 individuals as on May 30, 2020 as per the situation report published by World Health Organization (WHO)[2]. The accurate information about the emergence of COVID-19 is still unknown. But the initial cases have established links with the Huanan (Southern China) Seafood Wholesale Market[3,4]. The disease is contagious, and the virus gets spread amongst humans via respiratory droplets, physical contact, and also through fecal-oral transmission[5]. Numerous cases of pneumonia of unknown cause were reported in Wuhan, China in December 2019. The cases showed similar clinical characteristics with viral pneumonia[6]. The patients suffering from COVID-19 infection are observed to have serious pneumonia with abnormal observations on chest Computed Tomography (CT) examination[7]. The unavailability of medicine for this disease requires efficient diagnosis methods for controlling the disease.

Common cold to pneumonia is caused by a group of viruses known as CoV. These diseases include respiratory, enteric, renal, and neurological diseases. These viruses are grouped into four genres namely alpha-CoV, beta-CoV, gamma-CoV, and delta-CoV[8]. Figure 1 gives an overview of the disease.

The virus affects individuals from all age groups and genders. A research study reveals that two groups of people are specifically affected by this disease. The first group of individuals are those who are above 60 years old. The second group is of those individuals who have some underlying medical condition like diabetes, cardiovascular disease, and hypertension. The common symptoms of COVID-19 include fever, dry cough, and respiratory problems like shortness of breath, muscular soreness, and fatigue. In some cases, diarrhoea and vomiting are also reported. The severity of the disease ranges from mild flu to pneumonia causing respiratory ailments. The advance stage of the disease even causes organ failures and Acute Respiratory Distress Syndrome (ARDS) leading to the deaths of the patients. The fast-paced human to human transmission of the disease is a matter of great concern for the regulatory authorities globally. The control of COVID-19 largely depends on the diagnosis at the right time. The available methods for diagnosis comprise of laboratory tests like Reverse-Transcription Polymerase Chain Reaction (RT-PCR), real-time RT-PCR (rRT-PCR), and Reverse Transcription Loop-mediated isothermal Amplification (RT-LAMP) test[9,10]. The laboratory tests have some limitations. Firstly, the test requires testing kits which have limited availability in the supply chain. Secondly, the test is time consuming due to the laboratory processes involved. The X-Ray facilities are easily accessible in all parts of the world and the results are also produced at a fast pace. Therefore, the chest X-Ray images may be utilized for detecting the presence of COVID-19. The development of an automated method based on chest X-Ray images for support in clinical decision making will be significant for the disease control. According to WHO, the disease can be controlled by stopping the chain of transmission. Officials have reported that testing and isolation are the two key actions that are useful in breaking the chain of transmission. Therefore, the accurate diagnosis is significant in controlling COVID-19.

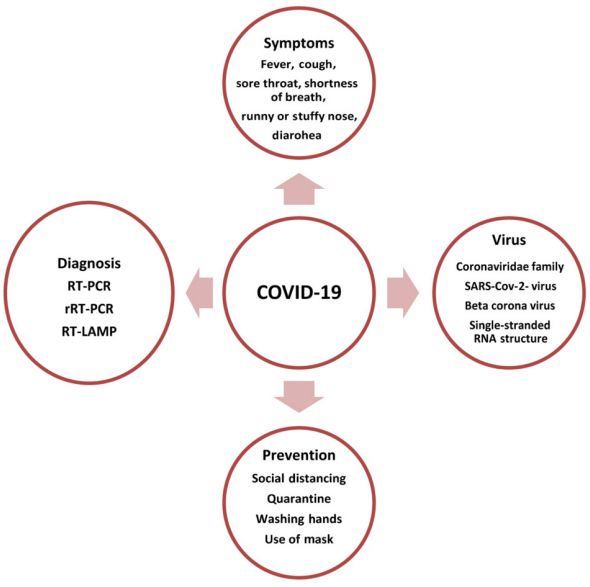

Fig. 1 Overview of COVID-19.

The detection of COVID-19 can be done at an earlier stage with chest images as compared to the PCR testing. The chest X-Ray images can be analyzed by using artificial intelligence techniques[11].

Numerous techniques for diagnosis of COVID-19 using machine learning techniques on radiological images are available in the literature. A transfer learning model for diagnosis of coronavirus from chest X-Ray images is presented in Ref. [12]. Another method with improved accuracy presented a segmentation-based approach. The method classified the input images as

normal, viral pneumonia, and COVID-19[13]. A deep learning-based model is applied on CT images for detection of COVID-19. Some researchers have also developed public datasets comprising of chest X-Ray images of COVID-19 patients[14, 15]. A method named COVID-Net is developed and applied on these public datasets for diagnosis of COVID-19[14]. The use of deep learning for diagnosis from the chest X-Ray images provides good results. Deep learning models are being widely used for medical image processing. In Ref. [16], the detection of pneumonia is done using convolution neural networks. In this paper, an automated method for the diagnosis of COVID-19 from a deep network is proposed. The proposed network utilizes the feature generated by multiresolution analysis. The combination of wavelet transforms along with the deep network brings multiple advantages. The wavelet decomposition is fed into the network. The network used is not the traditional Convolutional Neural Network (CNN). A depthwise separable network is utilized in this work.

2 Background

In this section, the wavelet technique and depthwise convolution neural network are discussed.

2.1 Wavelet

Wavelet theory is a transform-based image processing technique that makes use of Wavelet transforms. Wavelets are derived from small waves of changing frequency and limited duration[17]. These are useful as they provide both temporal as well as frequency information for images.

The 2D scaling functions, including $\varphi(x, y)$, $\psi^H(x, y)$, $\psi^V(x, y)$, and $\psi^D(x, y)$, are required for two-dimensional multiresolution analysis. All these scaling functions are obtained by multiplying the one-dimensional functions. The product of these produces four two-dimensional separable scaling function and separable "directionally sensitive" wavelets:

$$\varphi(x, y) = \varphi(x)\varphi(y) \tag{1}$$

$$\psi^H(x, y) = \psi(x)\varphi(y) \tag{2}$$

$$\psi^V(x, y) = \varphi(x)\psi(y) \tag{3}$$

$$\psi^D(x, y) = \psi(x)\psi(y) \tag{4}$$

These functions record the variance in horizontal, vertical, and diagonal directions. The separabilty in Eqs. (1)–(4) is the major cause of the directional sensitivity. The computational complexity of the 2D transform remains the same. The scaled and translated basis functions are defined as

$$\varphi_{j,m,n}(x, y) = 2^{j/2}\varphi(2^j x - m, 2^j y - n) \tag{5}$$

$$\psi^i_{j,m,n}(x, y) = 2^{j/2}\psi^i(2^j x - m, 2^j y - n), \quad i = \{H, V, D\} \tag{6}$$

The discrete wavelet transform of an image $f(x, y)$ of size $M \times N$ is

$$W_\varphi(j_o, m, n) = \frac{1}{\sqrt{MN}} \sum_{x=0}^{M-1} \sum_{y=0}^{N-1} f(x, y)\, \varphi_{j_o,m,n}(x, y) \tag{7}$$

$$W^i_\psi(j, m, n) = \frac{1}{\sqrt{MN}} \sum_{x=0}^{M-1} \sum_{y=0}^{N-1} f(x, y)\psi^i_{j,m,n}(x, y), \quad i = \{H, V, D\} \tag{8}$$

where j_o is an arbitrary starting scale and the $W_\varphi(j_o, m, n)$ coefficients define an approximation of $f(x, y)$ at scale j_o. $W^i_\psi(j, m, n)$ coefficients add horizontal, vertical, and diagonal details for scales greater than j_o. Generally, $j_o = 0$ is selected and $N = M = 2^j$ so that $j = 0, 1, 2, \ldots, j - 1$, and $m = n = 0, 1, 2, \ldots, 2^j - 1$.

Given W_φ and W^i_ψ of Eqs. (7) and (8), $f(x, y)$ is obtained by performing inverse discrete wavelet transform:

$$f(x, y) = \frac{1}{\sqrt{MN}} \sum_m \sum_n W_\varphi(j_o, m, n)\varphi_{j_o,m,n}(x, y) + \frac{1}{\sqrt{MN}} \sum_{i=H,V,D} \sum_{j=j_o}^{\infty} \sum_m \sum_n W^i_\psi(j, m, n)\psi^i_{j,m,n}(x, y) \tag{9}$$

2.2 Depthwise separable convolution neural network

The standard convolution layer of a neural network has large number of parameters. This leads to over fitting of the network. Depthwise convolution and depthwise separable convolution layers overcome this problem. These convolution layers reduce the computational cost as well as the number of parameters. The depthwise convolution layers can reduce the computational cost and the parameter space. The reduction in parameters in no way reduces the efficiency of the network. The standard convolution is divided into depthwise and pointwise convolution[18]. The depthwise convolution is responsible for applying convolution on every input. The output of depthwise convolution is merged using pointwise convolution. The l-th layer of the network having a 3D input tensor x^l such that

$x^l \in I^{H^l \times W^l \times D^l}$ where H, W, and D represent the height, weight, and depth of the input vector. The convolution layer output $(y_{i^{l+1}j^{l+1},d})$ represents the point at location (i, j) in d-th channel and $l + 1$ layer. This can be computed using

$$y_{i^{l+1}j^{l+1},d} = \sum_{d=0}^{D} f_d \times \sum_{i=0}^{H} \sum_{j=0}^{W} f_{i.j} \times x^l_{i^{l+1}j^{l+1},d} \tag{10}$$

where f_d is a pointwise filter of size 1×1.

The depthwise separable convolution performs the operation in two steps. In the first step, a depthwise convolution is applied on the input. Thereafter, the pointwise convolution is applied on the output of the depthwise convolution. The spatial correlations are obtained from depthwise convolution and the channel wise correlations are obtained from pointwise convolution. The combination of these two forms the feature map.

3 Proposed Method

The proposed method is based on depthwise separable convolution network and spectral pooling using wavelet transforms. The network is formulated by combining multiresolution analysis with deep learning. The traditional CNN layers suffer from over fitting and high computational cost due to large number of parameters generated at each layer. Powerful properties of the Discrete Wavelet Transform (DWT), spectral domain, spectral pooling, and spectral parameterization of convolutional layers are utilized as a means to improve CNNs by improving training convergence, allowing flexible pooling dimensions, and retaining or improving competitive classification accuracies.

The filters in the network learn from the spectral domain instead of the spatial domain. The low frequency spectrum of the input contains most of the details and the high frequency spectrum contains noise information. This non-uniformity of spectrum power enables the removal of high frequencies do minimal damage of input information. Spectral pooling truncates the spectral representation of an image–kernel product. Simply put, spectral pooling is simple low-pass filter. This technique is desirable because it can be combined with the convolution theorem to achieve fast training results. The convolution theorem states that convolution can be used considerably by being performed in the spectral domain as element-wise multiplication. The details of the proposed network are discussed in the following section. Given an image x, it can be divided into four subbands x_{LL}, x_{LH}, x_{HL}, and x_{HH} using the Discrete Wavelet transform with convolution filters f_{LL}, f_{LH}, f_{HL}, and f_{HH}. These filters have fixed parameters and a stride of 2. The stride of two provides the down sampling of the result obtained from convolution. These four sub-bands are fed into the depthwise separable network for further processing. The flow chart of the proposed method is shown in Fig. 2.

The proposed method comprises of the following steps:

(1) Input image: The COVID-19 dataset comprises of the chest X-Ray images. These images are used for the detection. The images are of different sizes, thus they are resized to $3 \times 224 \times 224$.

(2) Image normalization: The input images are normalized prior to any further processing. Normalized images are enhanced images with no errors due to lightening conditions.

(3) Image decomposition with wavelet: This step is one of the most significant steps that convert the spatial domain input to frequency domain. The input images are decomposed into four sub-bands. Haar Wavelet transform is used to decompose the image into sub bands. The dataset is augmented and split into training and testing set.

(4) Convolution layers: This step comprises of three standard convolution blocks. The input is convolved in these three blocks.

(5) Spectral pooling and batch normalization: Next layer is the pooling layer which combines the features from the output of the different layers. In this paper, average pooling is performed in which the convolution is followed by down sampling.

(6) Output layer: The next layer is the fully connected layer. The softmax optimizer is applied in the last layer to predict the output.

(7) Grad-CAM output visualization: The prediction output obtained from the network needs to be visualized for building trust on the network for making diagnosis decision. The Grad-CAM utilizes the gradient information from the last layer of the network to visually represent the class activation map.

(8) Diagnosis decision: Finally, any given input chest X-Ray image is classified into one of three classes, i.e., normal, COVID-19, or viral pneumonia.

The details of the network architecture are discussed in the following sections.

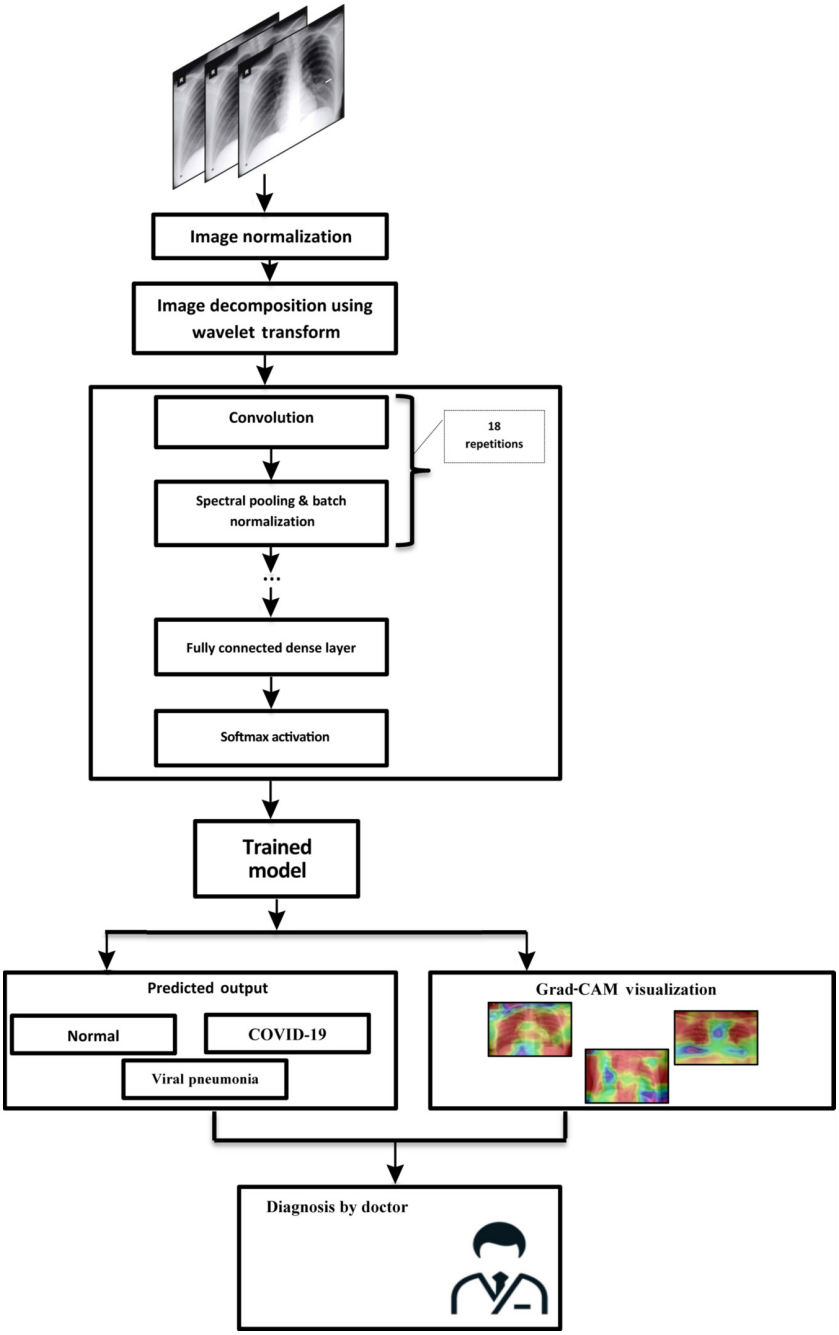

Fig. 2 Proposed methodology.

3.1 Network architecture

The input layer of the network is fed with chest X-Ray images. The network comprises of eighteen convolution layers. The network comprises of a mix of regular and depthwise convolution layers. The batch size is fixed to eight. There are six regular and twelve depthwise layers. Multiresolution analysis is integrated into the network after the first convolution block. Between the convolution layers, max pooling layers are added. The batch normalization layers are used to solve the local minima problem by mapping the activations to the mean of zero and unit variance. It also makes the convergence for the network fast[19]. The over fitting problem is solved by using a dropout of 0.2[20]. The specifications of the network layers are given in Table 1.

3.1.1 Convolution layer

Given an input vector with n components $\boldsymbol{X} = \{x_1, x_2, x_3, \ldots, x_n\} \in \mathbf{R}^n$, the output vector $\boldsymbol{Y} = \{y_1,$

Table 1 Model summary.

Layer type	Output shape	Number of parameters	Kernel size	Dropout	Number of filters
Input	(224, 224, 3)	0	–	0	–
Wavelet Lambda	(112, 112, 12)	0	3 × 3	0	4
Separable Conv 2dx2 (ReLU)	(14, 14, 256)	3436	3 × 3	0	32
Batch normalization	(14, 14, 256)	1024	–	0	–
Maxpooling 2d	(7, 7, 256)	0	–	0	–
Separable Conv 2dx2 (ReLU)	(7, 7, 256)	68 096	3 × 3	0	64
Batch normalization	(7, 7, 256)	68 096	–	0	–
Maxpooling 2d	(7, 7, 256)	0	–	0.2	–
Separable Conv 2dx2 (ReLU)	(7, 7, 256)	1024	3 × 3	0	128
Batch normalization	(7, 7, 256)	512	–	0	–
Maxpooling 2d	(7, 7, 256)	0	–	0.2	–
Separable Conv 2dx2 (ReLU)	(7, 7, 256)	102 272	3 × 3	0	256
Batch normalization	(7, 7, 256)	1024	–	0	–
Maxpooling 2d	(3, 3, 256)	0	–	0.2	–
Separable Conv 2dx2 (ReLU)	(3, 3, 256)	133 888	3 × 3	0	256
Batch normalization	(3, 3, 256)	1024	–	0	–
Maxpooling 2d	(3, 3, 256)	0	–	0.2	–
Separable Conv 2dx2 (ReLU)	(3, 3, 512)	267 264	3 × 3	0	512
Batch normalization	(3, 3, 512)	2048	–	0	–
Maxpooling 2d	(1, 1, 512)	0	–	0.2	–
FC1 (ReLU)	(512)	262 656		0.7	512
FC2 (ReLU)	(128)	65 664		0.5	128
FC3 (ReLU)	(64)	8256		0.3	64
FC4 (ReLU)	(32)	2080		0.2	32
FC5 (ReLU)	(3)	99		0	3

$y_2, y_3, \ldots, y_n\} \in \mathbf{R}^n$.

$$y_i = \sum_{j \in N_i} w_j x_j \tag{11}$$

where N_i is a set of indices of neighbours x_i and the weight w_j. The computation of y_i is equivalent to convolution operation of the input by the weight vector. Thus it can be written using the convolution operator $*$ as

$$y = x * w \tag{12}$$

where $w = (w_0, w_1, \ldots, w_{n-1}) \in \mathbf{R}^n$.

3.1.2 Pooling layer

After the convolution layer is the pooling layer. In this paper, average pooling is used in connection with multiresolution analysis. The output of the pooling layer is the vector with fewer number of components as compared to the input vector. The output of the pooling layer is defined as

$$y_j = \frac{1}{p} \sum_{k=0}^{p-1} x_{pj+k}, \quad y \in \mathbf{R}^m \tag{13}$$

where p is the support of pooling and $m = \dfrac{n}{p}$.

The value of p defines the value by which the number of parameters is reduced. For example, if the value of p is 3, then the number of parameters is reduced to one third by taking triplets in average. Pooling can be written in the form of down sampling as follows:

$$y = (x * p) \downarrow l \tag{14}$$

Average pooling performs convolution by p followed by down sampling by l.

3.2 Activation function

The activation function used is the ReLU function. Activation function is significant in the convergence of the network. ReLU is the rectified linear activation function, and is the most used activation function[21]. This function overcomes the vanishing gradient problem and makes the model more efficient and faster. Mathematically, it can be expressed as

$$f(x) = \max(0, x) \tag{15}$$

Thus, the function brings all negative values to zero whereas positive values remain as it. The ReLU function is used in the hidden layers. In the last layer, softmax activation function is used. The softmax function is

$$\text{Softmax}(x_i) = \frac{\exp(x_i)}{\sum_j \exp(x_j)} \tag{16}$$

where x_i is the observed output and divided by the sum of all possible output.

3.3 Training method

The training of the network is one of the most significant tasks. The weight vector of the network is updated to minimize the value of the cost function. The probabilities over the classes for classification are computed. The loss function used in this paper is categorical cross entropy[22]. The other important task in training is to balance the dataset. The data are balanced with the help of data augmentation. With data augmentation, new samples are generated. A rotation angle of -15 degrees to $+15$ degrees is used for augmenting the dataset. The optimization method used here is Adam optimization with weight decay. This leads to faster convergence and higher performance of the network. The other parameters are number of epochs which are chosen to be 100 and the batch size is set to 8. The model is evaluated using metrics like F1-score, precision, validation accuracy, sensitivity, specificity, etc., which is detailed in Section 5.

4 Dataset

The dataset used for the experiments comprises of chest X-Ray images of COVID-19, viral pneumonia patients, and healthy individuals. The annotated Post Anterior (PA) view of chest X-Ray images is used[23,24]. A total of 1439 images from the three classes are available in the dataset. The number of images of COVID-19 is 132; viral pneumonia is 629; and the number of images of normal case is 678. The images are of both males and females from all over the world. For model building process, we split the dataset into training and test set that 80% for training the model and 20% for validation purpose. Table 2 presents the distribution of the images present in the dataset. The sample images depicting normal, viral pneumonia, and COVID-19 patients are shown in Fig. 3[19].

Table 2 Distribution of images in train and test sets.

Image type	Train	Test
Normal	542	136
Viral pneumonia	503	126
COVID-19	106	26
Total	1151	288

5 Experiment and Result

The implementation of the proposed network is done using Keras library in Python. The experimental setup and results are presented in this section. The model was tuned to obtain the best results. The decomposition of the image was done using Haar wavelet transform. A total of twelve separable and six convolution layers are used. Adam optimizer with weighted decay is used for optimization of the network. The quantitative analysis of the results obtained is done using sensitivity, precision, and F1-score[25]. These metrics are computed using Eqs. (17) – (20). Sensitivity represents the correctness of classification. It can be computed as

$$\text{Sensitivity} = \frac{\text{TP}}{\text{TP} + \text{FN}} \times 100\% \tag{17}$$

The misclassifications are reported by precision. If there are no misclassifications, the precision will be 100%. F1-score is the harmonic mean of precision and sensitivity. The F1-score of value one represents perfect precision and sensitivity.

$$\text{Precision} = \frac{\text{TP}}{\text{TP} + \text{FP}} \times 100\% \tag{18}$$

$$\text{F1-score} = 2 \times \frac{\text{precision} \times \text{sensitivity}}{\text{precision} + \text{sensitivity}} \times 100\% \tag{19}$$

$$\text{Accuracy} = \frac{\text{TP} + \text{TN}}{\text{TP} + \text{TN} + \text{FP} + \text{FN}} \times 100\% \tag{20}$$

where TP, FP, and FN represent the true positive, false positive, and false negative, respectively. The confusion matrix for the three classes normal, COVID-19, and viral pneumonia is shown in Table 3. The values

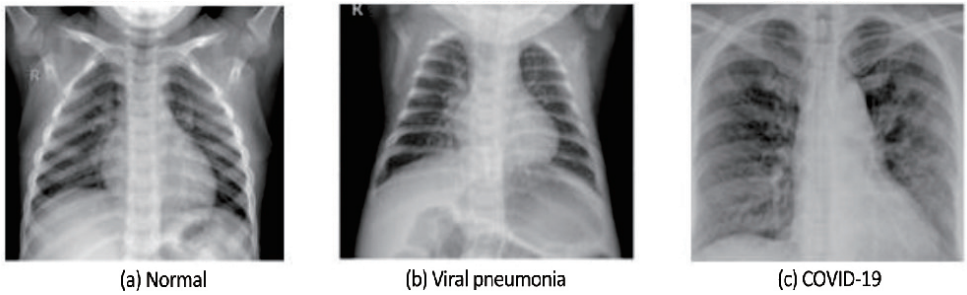

Fig. 3 Sample images of normal, viral pneumonia, and COVID-19 infected patients[9].

Table 3 Confusion matrix.

Disease type	Predicted result		
	Normal	COVID-19	Viral pneumonia
Normal	**130**	1	5
COVID-19	1	**24**	1
Viral pneumonia	**3**	**1**	**122**

obtained for the proposed method are summarized in Table 4.

Figure 4 shows the Grad-CAM for the three classes. The Grad-CAM visualization is used along with the classifier predictions for diagnosis of the disease accurately.

The performance of the proposed method is compared with other existing methods. The results are compared with four latest techniques that have used deep learning models for the diagnosis of COVID-19 using chest X-RAY images. The results are summarized in Table 5. The analyses of the results reveal that the proposed method outperforms the existing methods. DarkCovidNet uses You Only Look Once (YOLO) network with 17 layers for detection of COVID-19 from chest X-Ray images[26]. The performance of DarkCovidNet is average with an overall accuracy of approximately 87%. The second and third methods are based on EfficientNet[27]. Two variations of the method are presented namely flat and hierarchical. These two methods have an overall accuracy of approximately 93%. The DeTraC-ResNet18 performs better than these methods and has an overall accuracy of 95.12%. The proposed method has further improved the overall accuracy. The overall accuracy of the proposed method is 95.83%. The bar graph of the comparative study is shown in Fig. 5.

Table 4 Value for the proposed method. (%)

Disease type	Accuracy	Precision	Sensitivity	F1-score
Normal	96.53	97	96	96
COVID-19	98.61	92	92	92
Viral pneumonia	96.53	95	97	96

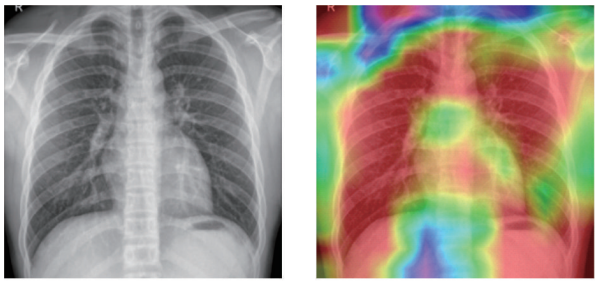

(a) Normal

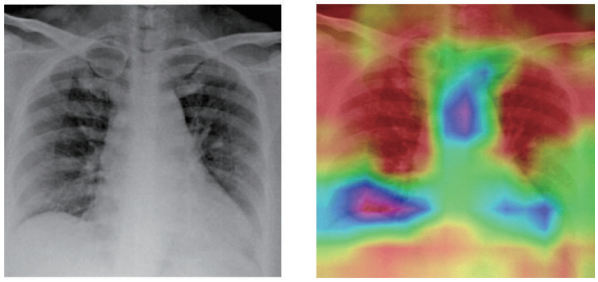

(b) COVID-19

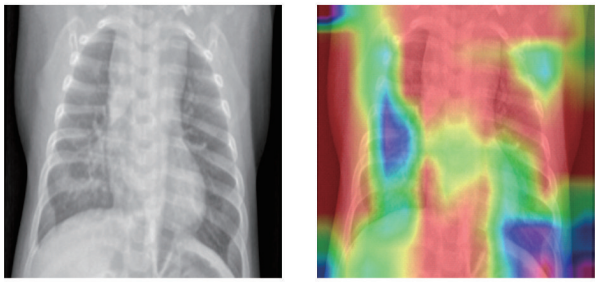

(c) Viral pneumonia

Fig. 4 Grad-CAM visualization of (a) normal, (b) COVID-19, and (c) viral pneumonia.

6 Conclusion

The paper presented an automated method for detection of COVID-19 from chest X-Ray images. An improved depthwise convolution network is designed that incorporates spectral analysis. The convolution and pooling layers are reformulated as a generalized case of filtering and down sampling. With this reformulation, multiresolution analysis is integrated with depthwise

Table 5 Comparative analysis. (%)

Method	Accuracy	Precision	Sensitivity	F1-score
DarkCovidNet	87.02	89.96	85.35	87.37
Flat-EfficientNet B3	93.34	93.93	93.96	93.94
Hierarchical-EfficientNet B3	93.51	93.93	93.55	93.73
DeTraC-ResNet18	95.12	93.36	97.91	95.58
Proposed	**95.83**	**95.67**	**96.07**	**95.63**

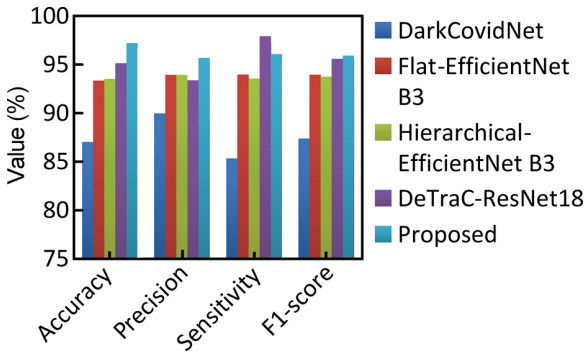

Fig. 5 Comparative study.

network. The input images are decomposed using Haar wavelet for multiresolution analysis. The wavelet is applied in the form of fixed weight filters. The developed model is applied on chest X-Ray images for detection of COVID-19 disease. The model classifies the images into three classes: normal, viral pneumonia, and COVID-19. A comparative study is also performed to evaluate the performance of the proposed method. The developed methodology can be used for diagnosis of COVID-19 from chest X-Ray images. The use of X-Ray images will help in controlling the disease.

References

[1] A. C. Walls, Y. J. Park, M. A. Tortorici, A. Wall, A. T. McGuire, and D. Veesler, Structure, function, and antigenicity of the SARS-CoV-2 spike glycoprotein, *Cell*, vol. 181, no. 2, pp. 281–292, 2020.

[2] World Health Organization, Coronavirus Disease 2019 (COVID-19), Situation Report–81, https://www.who.int/docs/default-source/coronaviruse/situation-reports/20200410-sitrep-81-covid-19.pdf, 2020.

[3] N. S. Chen, M. Zhou, X. Dong, J. M. Qu, F. Y. Gong, Y. Han, Y. Qiu, J. L. Wang, Y. Liu, Y. Wei, et al., Epidemiological and clinical characteristics of 99 cases of 2019 novel coronavirus pneumonia in Wuhan, China: A descriptive study, *Lancet*, vol. 395, no. 10 223, pp. 507–513, 2020.

[4] Q. Li, X. H. Guan, P. Wu, X. Y. Wang, L. Zhou, Y. Q. Tong, R. Q. Ren, K. S. M. Leung, E. H. Y. Lau, J. Y. Wong, et al., Early transmission dynamics in Wuhan, China, of novel coronavirus–infected pneumonia, *New England Journal of Medicine*, vol. 382, no. 13, pp. 1199–1207, 2020.

[5] J. F. W. Chan, S. F. Yuan, K. H. Kok, K. K. W. To, H. Chu, J. Yang, F. F. Xing, J. L. Liu, C. C. Y. Yip, R. W. S. Poon, et al., A familial cluster of pneumonia associated with the 2019 novel coronavirus indicating person-to-person transmission: A study of a family cluster, *Lancet*, vol. 395, no. 10 223, pp. 514–523, 2020.

[6] D. W. Wang, B. Hu, C. Hu, F. F. Zhu, X. Liu, J. Zhang, B. B. Wang, H. Xiang, Z. S. Cheng, Y. Xiong, et al., Clinical characteristics of 138 hospitalized patients with 2019 novel coronavirus–infected pneumonia in Wuhan, China, *JAMA*, vol. 323, no. 11, pp. 1061–1069, 2020.

[7] C. L. Huang, Y. M. Wang, X. W. Li, L. L. Ren, J. P. Zhao, Y. Hu, L. Zhang, G. H. Fan, J. Y. Xu, X. Y. Gu, et al., Clinical features of patients infected with 2019 novel coronavirus in Wuhan, China, *Lancet*, vol. 395, no. 10 223, pp. 497–506, 2020.

[8] X. Y. Ou, Y. Liu, X. B. Lei, P. Li, D. Mi, L. L. Ren, L. Guo, R. X. Guo, T. Chen, J. X. Hu, et al., Characterization of spike glycoprotein of SARS-CoV-2 on virus entry and its immune cross-reactivity with SARS-CoV, *Nature Communications*, vol. 11, p. 1620, 2020.

[9] P. Zhai, Y. B. Ding, X. Wu, J. K. Long, Y. J. Zhong, and Y. M. Li, The epidemiology, diagnosis and treatment of COVID-19, *International Journal of Antimicrobial Agents*, vol. 55, no. 5, p. 105 955, 2020.

[10] X. Z. Xie, Z. Zhong, W. Zhao, C. Zheng, F. Wang, and J. Liu, Chest CT for typical 2019-nCoV pneumonia: Relationship to negative RT-PCR testing, *Radiology*, vol. 296, no. 2, p. 200 343, 2020.

[11] D. S. Kermany, M. Goldbaum, W. J. Cai, C. C. S. Valentim, H. Y. Liang, S. L. Baxter, A. McKeown, G. Yang, X. K. Wu, F. B. Yan, et al., Identifying medical diagnoses and treatable diseases by image-based deep learning, *Cell*, vol. 172, no. 5, pp. 1122–1131, 2018.

[12] S. Wang, B. Kang, J. L. Ma, X. J. Zeng, M. M. Xiao, J. Guo, M. J. Cai, J. Y. Yang, Y. D. Li, X. F. Meng, et al., A deep learning algorithm using CT images to screen for Corona Virus Disease (COVID-19), https://doi.org/10.1101/2020.02.14.20023028, 2020.

[13] X. W. Xu, X. G. Jiang, C. L. Ma, P. Du, X. K. Li, S. Z. Lv, L. Yu, Y. F. Chen, J. W. Su, G. J. Lang, et al., Deep learning system to screen coronavirus disease 2019 pneumonia, arXiv preprint arXiv: 2002.09334, 2020.

[14] J. P. Cohen, P. Morrison, and L. Dao, COVID-19 image data collection, arXiv preprint arXiv: 2003.11597, 2020.

[15] O. Gozes, M. Frid-Adar, H. Greenspan, P. D. Browning, H. Q. Zhang, W. B. Ji, A. Bernheim, and E. Siegel, Rapid AI development cycle for the coronavirus (COVID-19) pandemic: Initial results for automated detection & patient monitoring using deep learning CT image analysis, arXiv preprint arXiv: 2003.05037, 2020.

[16] D. Varshni, K. Thakral, L. Agarwal, R. Nijhawan, and A. Mittal, Pneumonia detection using CNN based feature extraction, in *Proc. 2019 IEEE Int. Conf. Electrical, Computer and Communication Technologies* (*ICECCT*), Coimbatore, India, 2019, pp. 1–7.

[17] A. Mehrotra and K. K. Singh, Detection of 2011 Tohoku tsunami induced changes in Rikuzentakata using normalized wavelet fusion and probabilistic neural network, *Disaster Advances*, vol. 7, no. 2, pp. 1–8, 2014.

[18] F. Chollet, Xception: Deep learning with depthwise separable convolutions, in *Proc. 2017 IEEE Conf. Computer Vision and Pattern Recognition* (*CVPR*), Honolulu, HI, USA, 2017, pp. 1800–1807.

[19] K. K. Singh, M. Siddhartha, and A. Singh, Diagnosis of Coronavirus Disease (COVID-19) from Chest X-Ray images using modified XceptionNet, *Romanian Journal of Information Science and Technology*, vol. 23, no. S, pp. S91–S115, 2020.

[20] N. Srivastava, G. Hinton, A. Krizhevsky, I. Sutskever, and R. Salakhutdinov, Dropout: A simple way to prevent neural networks from overfitting, *The Journal of Machine Learning Research*, vol. 15, no. 1, pp. 1929–1958, 2014.

[21] A. F. Agarap, Deep learning using rectified linear units (ReLU), arXiv preprint arXiv: 1803.08375, 2018.

[22] A. Mikolajczyk and M. Grochowski, Data augmentation for improving deep learning in image classification problem, presented at 2018 Int. Interdisciplinary PhD Workshop (IIPhDW), Swinoujście, Poland, 2018, pp. 117–122.

[23] J. P. Cohen, P. Morrison, and L. Dao, COVID-19 image data collection, arXiv preprint arXiv: 2003.11597, 2020.

[24] D. Kermany, K. Zhang, and M. Goldbaum, Labeled

Optical Coherence Tomography (OCT) and Chest X-Ray Images for Classification, https://data.mendeley.com/datasets/rscbjbr9sj/2, 2018.

[25] A. Ben-David, Comparison of classification accuracy using Cohen's Weighted Kappa, *Expert Systems with Applications*, vol. 34, no. 2, pp. 825–832, 2008.

[26] A. Abbas, M. M. Abdelsamea, and M. M. Gaber, Classification of COVID-19 in chest X-ray images using DeTraC deep convolutional neural network, arXiv preprint arXiv: 2003.13815, 2020.

[27] E. Luz, P. L. Silva, R. Silva, L. Silva, G. Moreira, and D. Menotti, Towards an effective and efficient deep learning model for COVID-19 patterns detection in X-ray images, arXiv preprint arXiv: 2004.05717, 2020.

Krishna Kant Singh is an associate professor in electronics & communication engineering at KIET Group of Institutions, Delhi-NCR, India. He is a senior member of IEEE. He has wide teaching and research experience. He has acquired BTech, MTech, and PhD (IIT Roorkee) degrees in the area of deep learning and remote sensing. He has authored more than 70 technical books and research papers in international conferences and SCIE journals of repute. He is the associate editor of *IEEE Access* and *Journal of Intelligent & Fuzzy System*. He is also the editorial board member of *Applied Computing and Geosciences*.

Akansha Singh is an associate professor in computer science engineering at Amity University Uttar Pradesh, Noida, India. She has wide teaching and research experience. She has acquired BTech, MTech, and PhD (IIT Roorkee) degrees in the area of neural network and remote sensing. She has authored more than 70 technical books and research papers in international conferences and SCIE journals of repute. Her area of interest includes mobile computing, artificial intelligence, deep learning & amp, and digital image processing. She is the associate editor of *IEEE ACCESS* and the guest editor of *Open Computer Science*.